Phase-Noise-Driven Instability in a Single-Mode Microchip Nd:YVO_4 Laser With Feedback

Tsong-Shin Lim, Tsung-Hsun Yang, Jyh-Long Chern, and Kenju Otsuka, *Fellow, IEEE*

***Abstract*—We report the instability behaviors of a single-mode microchip solid-state laser subjected to external feedback. Two kinds of instabilities, random chaotic burst generations and random sinusoidal burst generations, were observed experimentally in an LD-pumped microchip Nd:YVO_4 single-mode solid-state laser with fiber feedback. These results are totally different form those observed in laser diodes with delay feedback systems, which have been widely studied in last decades. Main features were reproduced numerically by utilizing the Lang–Kobayashi equations with phase noise, indicating phase-noise-driven dynamic instabilities.**

***Index Terms*—Laser stability, neodymium, numerical analysis, optical feedback, phase noise, solid lasers, stochastic differential equations.**

I. Introduction

IN HISTORY, the issue of instabilities in the output of lasers that are subjected to external feedback was initiated by the pioneering work of Lang and Kobayashi in 1980 [1]. They demonstrated the dynamic instabilities in a laser diode with external feedback which feature sustaining relaxation oscillations (ROs). They also confirmed theoretically that the dynamical instabilities take place in the transition process where the lasing frequency changes from one external cavity eigenmode to another in a weak-coupling regime. Thereafter, three universal transition routes to chaos, low-frequency fluctuations, and coherence collapse have been observed in LDs with external optical feedback for different feedback strength and/or delay time [2].

Some recent studies on the influence of optical feedback on LDs have focused on reducing or controlling the destabilizing effects of feedback [3]–[7]. Very weak feedback from short external cavities can significantly reduce both intensity noise and lasing linewidth [8]. The emission frequency can also be stabilized with phase-conjugate feedback [9]. On the other hand, variation of the feedback within the range that leads to chaotic operation can be used to encrypt information [10], [11]. Furthermore, feedback into a broad-area laser can bias the selection of a particular lateral mode, though this is sensitive to very small variations of the external-cavity length [12], [13]. Meanwhile, pulse-to-pulse jitter in spontaneously pulsing or externally switched LDs can be reduced with optical feedback, but the reduction is also extremely sensitive to small variations in cavity length [14], [15]. In contrast, studies on LD-pumped solid-state lasers with external optical feedback are still scant. Because LD-pumped solid-state lasers have been widely used in practical applications, it is important to clarify their dynamical behaviors both for academic and application reasons. Fiber linking capability of microchip lasers could be an important issue for practical applications. Thus, a characterization of the dynamics behind fiber-feedback-induced instability is crucial.

The time scales of the intensity fluctuations of LDs are much less convenient for precise dynamical measurements than those of solid-state lasers. Because the characteristic frequencies of solid-state lasers are sub-MHz, they are much more convenient for measurement. They also exhibit extremely high-sensitive responses to external feedback. The reason is that the cavity round-trip time τ_L ($\propto \tau_S$: photon lifetime) compared with the fluorescent lifetimes τ_f is extremely short [16]. Generally, the lifetime ratio $K = \tau_f/\tau_S$ of solid-state lasers ranges from 10^5 to 10^7, while $K \sim 10^3$ in LDs. Hence solid-state lasers become another promising laser systems for investigating the instabilities in lasers with delay feedback. Because the time scales of solid state lasers are dramatically different from those of LDs, the dynamical behaviors are expected to be unique. In fact, in the early experiment in which a microchip LNP ($LiNdP_4O_{12}$) solid-state laser was subjected to external feedback [17], feedback-induced random chaotic burst generations were observed. However, the instability is only observed in the regime of two lasing modes. Most recently, the random chaotic burst state has been re-examined using an LD-pumped LNP laser coupled to a single-mode optical fiber in a weakly-coupled regime, in which only one of the external cavity modes interacts with the solitary mode. It is conjectured that mode-partition noise in multimode regimes plays an essential role for producing the random chaotic burst state since phase fluctuation (FM) noise is extremely small in single-mode LNP lasers [18].

The results of the solid-state laser experiments cannot be interpreted in the context of low-frequency fluctuations in LDs described by the single-mode Lang–Kobayashi equations. Low-frequency fluctuations occur for moderate feedback when the laser is biased near the solitary laser threshold ($I/I_{\rm th} < 1.2 \sim 1.4$). In this regime, successively the laser intensity suddenly drops toward zero and gradually recovers with apparently random time length. The physical mechanism

Manuscript received March 13, 2001; revised May 24, 2001. This work was supported in part by the National Science Council, Taiwan, R.O.C., under Project NSC89-2112-M-006-023. The work of K. Otsuka was supported in part by the Monbusho International Scientific Research Program: Joint Research 10044175.

T.-S. Lim and J.-L. Chern are with the Department of Physics, National Cheng Kung University, Tainan 70101, Taiwan (e-mail: tslim@phys.ncku.edu.tw).

T.-H. Yang is with the Institute of Electro-Optical Engineering, National Chiao Tung University, Hsinchu 300, Taiwan.

K. Otsuka is with the Department of Applied Physics, Tokai University, Kanagawa 259-1292, Japan.

Publisher Item Identifier S 0018-9197(01)07370-5.

behind low-frequency fluctuations is still not fully understood, though several different explanations have been proposed. Mørk, Tromborg, and Christiansen explained low-frequency fluctuations as the result of bistability among the steady-state solutions introduced by the external cavity, i.e., external cavity modes [19]. Hohl, van der Linden, and Roy showed that spontaneous emission noise plays an important role in the nature and the statistics of the dropouts [20]. The experimental measurements agreed with those of Henry and Kazarinov, suggesting that spontaneous emission noise induces the dropout events [21]. On the other hand, Sano explained the dropouts as a result of a self-induced switching among distinct regions of phase space [22]. In Sano's interpretation, the laser moves toward the mode with maximum gain via chaotic itinerancy. However, since in the neighborhood of the maximum gain mode (stable external cavity mode) and antimodes (i.e., unstable external cavity modes) are very close, when the trajectory approaches an antimode, it is expelled into another region of phase space, and then starts moving toward the maximum gain mode again [23], [24]. Recent high-speed measurements on low-frequency fluctuations indicated that "power dropout" are seen as the envelope of a series of short pulse with 100 ps or less pulsewidth [24]. Similar pulses have been found in the Lang–Kobayashi model [23], [24]. In the meantime, temporally resolved optical spectra reveal that there is enhanced power in several longitudinal modes during the power dropout [25].

However, as will be shown below, the dynamical features of the instability of LD-pumped solid-state lasers with optical feedback are totally different from the instabilities (low-frequency fluctuations) in LDs. The instabilities reported below occur even in high pumping levels rather than near threshold only. On the other hand, instability occurs even with very weak feedback strength in which basically only one of the external cavity modes interacts with the solitary laser mode.e precisely, a variable attenuator was inserted.

In this paper, we report two kinds of random switching in an LD-pumped microchip neodymium-doped yttrium orthvanadate (Nd:YVO_4) single-mode laser coupled to a single-mode fiber. Two kinds of instabilities were observed in different feedback strength regimes, though the threshold reduction caused by feedback is less than 1%. In the weaker feedback regime, the laser output randomly switches between noise-driven relaxation oscillation and chaotic spike oscillation operations. In the stronger feedback regime (but the threshold reduction is still less than 1%), the laser output randomly switches between noise-driven relaxation oscillation and large-amplitude sinusoidal oscillation operations. The distinct features which are different from previous results are that the random burst generations were observed in a single-mode regime while in LNP lasers they were restricted to the multi-mode regime [17], [18] and the random chaotic burst occurred independently of the pump power level in weakly-coupled regimes in which only a single external cavity mode exists while low-frequency fluctuations in LDs has been observed only in the vicinity of solitary laser threshold in which many external cavity modes were involved in the dynamics. This paper is organized as follows. In Section II, the experimental scheme is described. The coupling coefficient is provided based on an estimate according to our experiment setup and main characteristics of the solitary Nd:YVO_4 laser are first summarized. The experimental results are presented in Section III. The random chaotic burst and the random sinusoidal burst are reported and their characteristic features are discussed. To explore experimental results, we utilize the Lang–Kobayashi equations including strong phase noise in numerical simulation and the observed random chaotic burst instability can be well reproduced as shown in Section IV. It is worthwhile to note that we employed time scales involving dynamics in microchip solid-state lasers, i.e., fluorescent lifetime, photon lifetime, and delay time, which are totally different from LDs. Section V describes the conclusions of our work.

II. Experimental Setup

The experimental setup is shown in Fig. 1. An LD-pumped microchip Nd:YVO_4 laser operated in the *single-mode* regime was employed and a compound cavity was formed with a single-mode fiber. The laser crystal (CASIX DPO3104; 1 mm thick, $1\%Nd^{3+}$ doped, and $5 \pm 2\%$ output coupling at 1064 nm) was inserted into a 2-mm-thick copper mount and its temperature was controlled at 25°C by a temperature controller. The pump beam of $\lambda_p = 808$ nm from the temperature-controlled LD was focused onto the laser crystal with a GRIN lens (0.22 pitch). The pumping threshold was around 40 mW and single-mode operation ranged up to 100 mW. Above 100 mW, the laser operates in a multi-mode regime (two modes and three modes were observed for different pumping powers). We also used a noise filter to eliminate the pumping noise caused by the LD controller and an interference filter to reduce the influence of pumping light on detection. In the entire pumping domain a linear π-polarized TEM_{00} mode of laser output was observed. The mode suppression ratio of the polarization mode is about 1/300. The laser beam was divided into two by a 50%-50% beamsplitter plate following after the interference filter. One was for measurement and the other was for feedback. We used a single-mode fiber (operating wavelength 1060 nm, core/cladding diameter 6.4/125 μm, cutoff wavelength 970 ± 60 μm, maximum attenuation 2.0 dB/km) as the feedback reflector such that the laser light reflected back from the far end of the fiber, in which the maximum field reflectivity is about 0.2. The coupling efficiency of the laser light into the fiber is estimated to be about 50%. To control the feedback strength more precisely, a variable attenuator was inserted.

The feedback strength can be estimated by threshold reduction. But to further quantify weak feedback, threshold reduction is not significant. Thus, we use alternative to handle the issue. The coupling coefficient κ can be estimated with the formula [26]

$$\kappa = \frac{r_{\text{ext}}}{\tau_L r_o}(1 - |r_o|^2). \tag{1}$$

where

- τ_L laser cavity round-trip time and is about 1.33×10^{-11} s for a 1-mm-thick Nd:YVO_4 chip (the index of refraction: $n_o = 1.9573$);
- r_o field reflectivity of the laser output mirror (about 0.975 for high-reflection coated);
- r_{ext} total field reflectivity of external components.

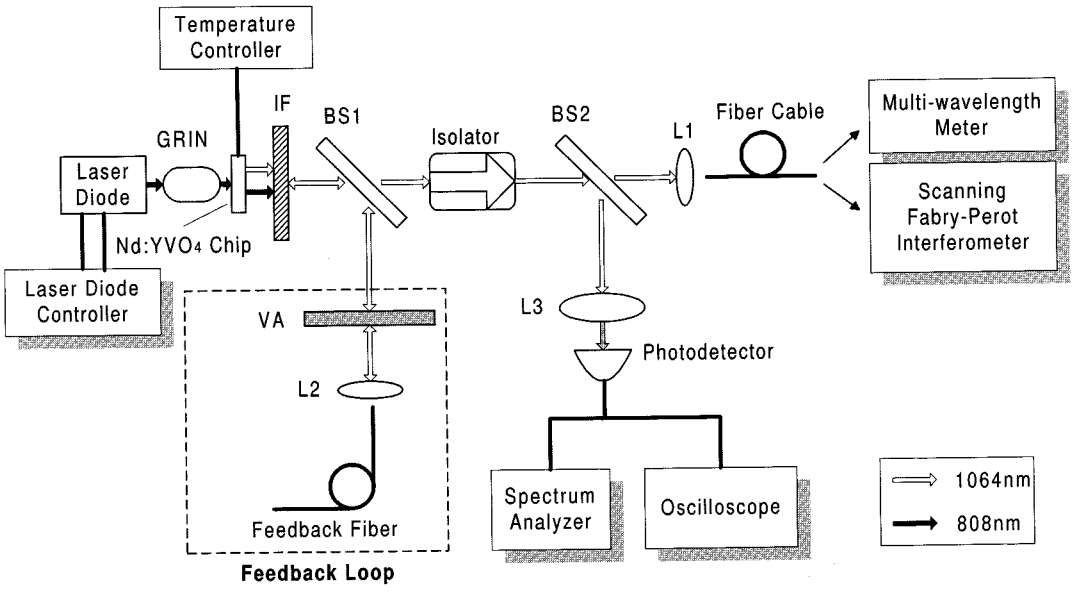

Fig. 1. Experimental setup. L1, L2: lens. BS1, BS2, BS3: beam splitter. GRIN: GRIN lens. IF: interference filter. VA: variable attenuator. Solid arrows indicate the 808-nm pumping beam and the empty arrows indicate the 1064-nm laser light from the Nd:YVO_4 laser.

Referring to the experimental setup, r_{ext} can be estimated as $r_{\text{ext}} = r_{bs} \cdot t_a \cdot \eta_c \cdot r_{f-a} \cdot t_a \cdot r_{\text{bs}}$. Here , r_{bs} is the field reflectivity of the beam splitter and is about 0.7 for a 50%–50% beam splitter. t_a is the transmission coefficient of the variable attenuator and the value is variable from 0 to 0.95. η_c is the coupling efficiency into the fiber. r_{f-a} is the field reflectivity of the the fiber–air interface and the value is about 0.2. Hence, the coupling coefficient κ is smaller than 1.7×10^8 s^{-1}. We will use this parameter κ to quantify our experiment.

In measurement, a multi-wavelength meter (resolution of 20 GHz) was employed to monitor the variation of the lasing mode. The single solitary mode operation was confirmed. The lasing wavelength λ_0 was 1064.245 nm. In the following experiment, single mode operation was maintained. A high-resolution scanning Fabry–Perot interferometer (resolution of 0.185 MHz) was used to identify the detailed structure of the oscillation spectrum of the laser output. The Nd:YVO_4 laser always emits a linearly polarized light due to the strong fluorescence anisotropy. The beamsplitter plate we used did not affect the polarization of laser light. The linear polarization was confirmed to be maintained after passing through the optical fiber because the fiber length was 10 m at most. Because the system was very sensitive to optical feedback, a Faraday isolator (isolation of 60 dB) was employed to isolate the feedback light from measurement part. We utilized a low-noise photodetector (typical rise time: < 1 ns) for detection and connected it to a transient oscilloscope (bandwidth: 500 MHz) for data acquisition. The GPIB interface was implemented to catch data from the oscilloscope with PC. An RF spectrum analyzer (bandwidth: 9 kHz–1.8 GHz) was used to monitor the behavior of laser output in the RF spectrum domain.

For comparison, typical output characteristics of the solitary Nd:YVO_4 laser are shown in Fig. 2, where the pumping power was 88 mW. In the absence of feedback, as shown in Fig. 2(a), the laser output exhibits noise-driven relaxation oscillation. The

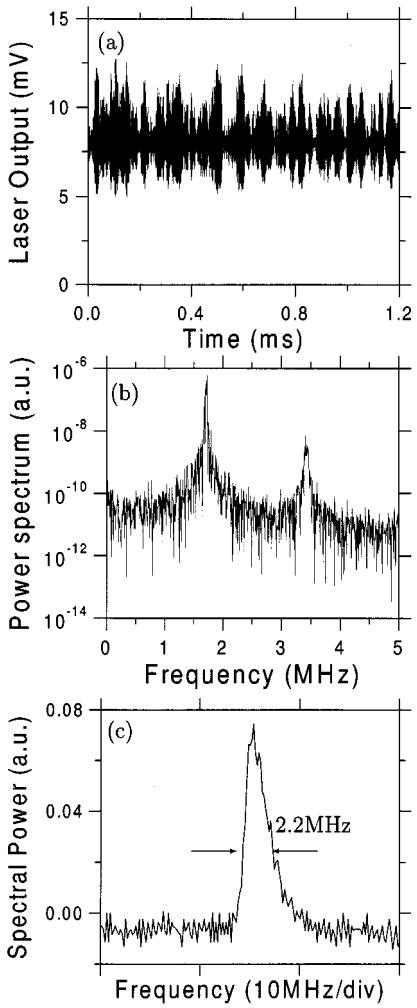

Fig. 2. Typical output characteristics of the solitary Nd:YVO_4 laser. (a) Temporal waveform. (b) Power spectrum. (c) Oscillation spectrum.

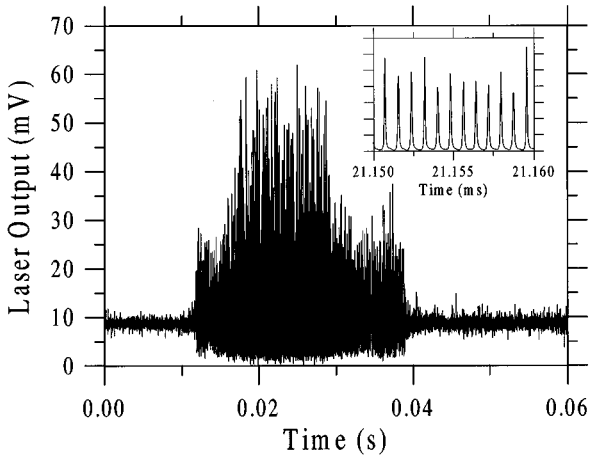

Fig. 3. Temporal waveform of random chaotic burst ($\kappa = 5.8 \times 10^6$ s^{-1}). The insert shows the short temporal trace of the chaotic spike oscillation part.

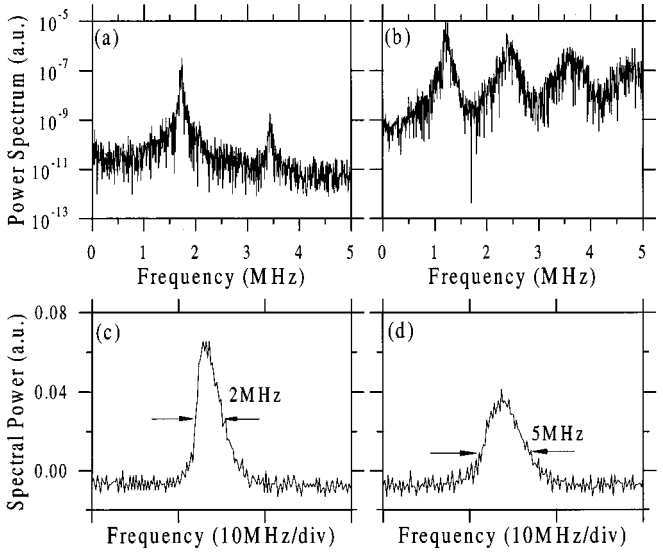

Fig. 4. The corresponding power spectra and oscillation spectra of Fig. 3. (a), (c) The noise-driven relaxation oscillation. (b), (d) The chaotic spike oscillation. The arrows in (c) and (d) indicate the FWHM linewidth.

corresponding power spectrum is shown in Fig. 2(b). The RO frequency, f_{RO}, is around 1.7 MHz and its second harmonic is at about 3.4 MHz. The oscillation characteristics were identified by utilizing the high-resolution scanning Fabry–Perot interferometer. In Fig. 2(c), the corresponding oscillation spectrum is presented and the full-width at half-maximum (FWHM) linewidth of the laser is estimated to be 2.2 MHz. Hereafter, the linewidth is denoted based on FWHM. As the pumping power was increased, the relaxation oscillation frequency increased following the $2\pi f_{RO} \propto \sqrt{(P/P_{\rm th}-1)/\tau_S\tau_f}$ relation, where P and $P_{\rm th}$ denote the pumping power and the threshold pumping power, respectively.

Several of the other optical properties of the Nd:YVO_4 crystal we used in our experiments are: diode-pumped optical-to-optical efficiency was $> 60\%$; fluorescent lifetime $\tau_f = 90$ μs; absorption coefficient $= 31.4$ cm^{-1}; absorption length $= 0.32$ mm; gain bandwidth $= 0.96$ nm (257 GHz); intrinsic loss $= 0.02$ cm^{-1}; stimulated emission cross-section $= 2.5 \times 10^{-18}$ cm^2.

III. General Features of the Experimental Results

A. Weaker Feedback Strength ($\kappa < 2.5 \times 10^7$ s^{-1})

We fixed the pumping power at 88 mW in all our experiments. In the presence of fiber feedback and when $\kappa < 1.1 \times 10^5$ s^{-1}, the dynamic features are almost the same as those of the solitary laser. When $\kappa > 1.1 \times 10^5$ s^{-1}, random chaotic burst occurs. A typical temporal waveform of random chaotic burst is shown in Fig. 3 for $\kappa \approx 5.8 \times 10^6$ s^{-1} with a 5-m fiber. The laser output randomly switches between noise-driven relaxation oscillation and chaotic spike oscillation. The duration time of chaotic spike oscillation is also irregular. The insert shows the short temporal trace of chaotic spike oscillation. Here, the irregular spiking oscillation waveform can be seen and has been identified to be chaos based on singular value decomposition analysis [27]. The power spectrum of noise-driven relaxation oscillation is shown in Fig. 4(a). This figure exhibits a typical noise-driven relaxation oscillation power spectrum with f_{RO} being also around 1.7 MHz. Fig. 4(b) shows the power spectrum of chaotic spike oscillation. One can see that the main frequency component shifts to a lower value (around 1.2 MHz) and the spectrum broadens. In the transition region, which shows the evolution from noise-driven relaxation oscillation to chaotic spike oscillation, the power spectrum broadens and the main frequency component shifts from f_{RO} to a lower frequency value which partially reflects the nature of chaotic spike oscillation.

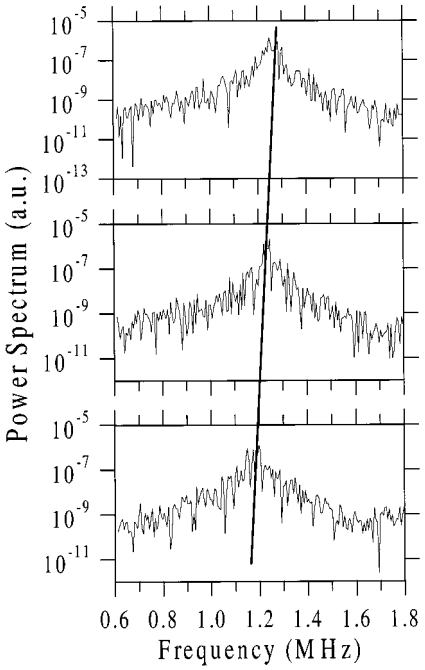

Fig. 5. Power spectra of chaotic spike oscillation with different feedback strengths. (a) $\kappa = 1.1\times10^6$ s^{-1}. (b) $\kappa = 5.2\times10^6$ s^{-1}. (c) $\kappa = 6.8\times10^6$ s^{-1}.

If we increase the feedback strength further, the f_{RO} of noise-driven relaxation oscillation, together with the dominant frequency of the chaotic spike oscillation, will shift to lower frequency values. Fig. 5 shows the power spectra of chaotic spike oscillation with different feedback strengths, $\kappa = 1.1\times10^6$ s^{-1},

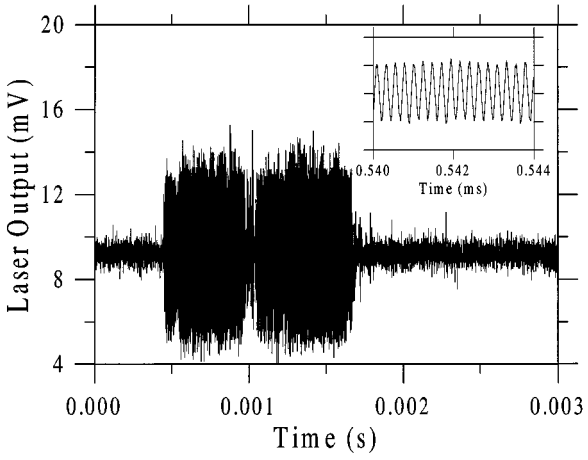

Fig. 6. Temporal waveform of random sinusoidal burst ($\kappa = 5.5 \times 10^7$ s^{-1}). The insert shows the short temporal trace of large-amplitude sinusoidal oscillation.

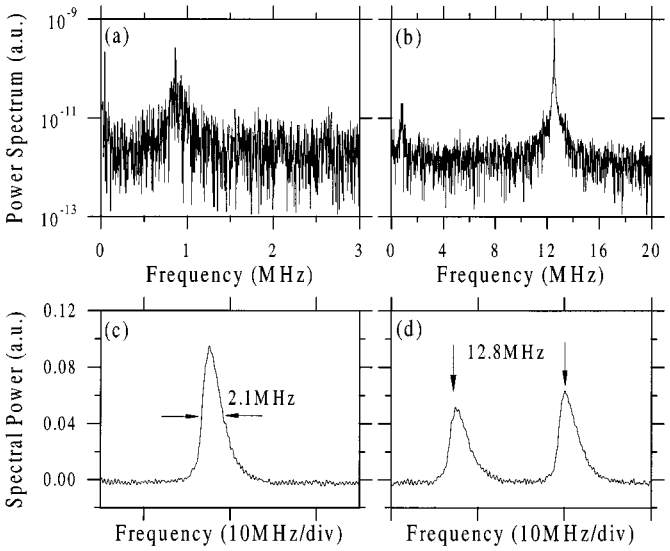

Fig. 7. The corresponding power spectra and oscillation spectra of Fig. 6. (a), (c) The noise-driven relaxation oscillation. (b), (d) The large-amplitude sinusoidal oscillation. In (d), the frequency difference between two modes is indicated by the down arrows with a value of 12.8 MHz.

5.2×10^6 s^{-1}, and 6.8×10^6 s^{-1}. The main frequency component shifts to lower values slightly due to the increase of the feedback strength as indicated by the line crossing the figures. The range of the frequency shift in this regime is about 0.2 MHz. This feature differs from the previous results in LDs that f_{RO} increases with a increase of feedback strength [28]. As will be discussed below, this is due to the time scale difference between LDs and solid-state lasers.

By utilizing a high-resolution scanning Fabry–Perot interferometer with suitable triggering, we can characterize the linewidth of the laser output in different regions. As shown by Fig. 4(c), the linewidth corresponding to noise-driven relaxation oscillation in Fig. 3 is about 2 MHz which is close to that of the solitary laser. On the other hand, Fig. 4(d) shows the corresponding oscillation spectrum of chaotic spike oscillation of Fig. 3, and the linewidth broadens to about 5 MHz. Because the lasing linewidth is mainly due to the phase fluctuation, this implies that the phase fluctuation becomes larger as chaotic spike oscillation occurs.

B. Stronger Feedback Strength ($2.5\times10^7 < \kappa < 1.7\times10^8$ s^{-1})

For stronger feedback strength, i.e., $\kappa > 2.5 \times 10^7$ s^{-1}, another kind of burst was observed and the burst mentioned in Section III–A disappeared. For $\kappa \sim 2.5 \times 10^7$ s^{-1}, these two different bursts can coexist. In Fig. 6, the output waveform observed at $\kappa = 5.5 \times 10^7$ s^{-1} is shown. Here, random sinusoidal burst is observed. The laser output randomly switches between noise-driven relaxation oscillation and large-amplitude sinusoidal oscillation, and the duration time of large-amplitude sinusoidal oscillation is also irregular. The insert shows the short temporal trace of large-amplitude sinusoidal oscillation. The large-amplitude oscillation exhibits a sinusoidal waveform. The corresponding power spectra of Fig. 6 are shown in Fig. 7. Fig. 7(a) shows the power spectrum of noise-driven relaxation oscillation. f_{RO} is shifted by ~0.9 MHz to a lower frequency value due to stronger optical feedback. In contrast, as shown in Fig. 7(b), which is corresponds to large-amplitude sinusoidal oscillation, a sharp peak which denotes the frequency of the sinusoidal waveform is found at about 12.5 MHz. Its value increases with an increase of the feedback strength and the range of the frequency shifting will be discussed latter.

Next, we report the oscillation spectra in this regime. In contrast to weaker feedback strength (i.e., $\kappa < 2.5 \times 10^7$ s^{-1}), in which only linewidth broadening was observed, a random switching between single-mode and two-mode operations was observed. Figs. 7(c) and (d) show the corresponding oscillation spectra of Fig. 6. Fig. 7(c) shows the single-mode operation with a linewidth of 2.1 MHz, which approximates that of the solitary laser. Fig. 7(d) shows the case of two-mode operation. The oscillation frequency difference between two modes is about 12.8 MHz, as indicated by the down arrows. This value also approximates the frequency of the sinusoidal waveform. In this regime, the frequency of the sinusoidal waveform and the oscillation frequency difference between two observed modes are approximately equal and vary with the feedback strength.

To explore the influence of delay time (fiber length) on the experimental results, we further used two additional fibers with different lengths of 10 and 2 m. In the weaker feedback regime, $\kappa < 2.5 \times 10^7$ s^{-1}, the dynamical features are almost the same as those of the 5-m fiber. However, in the stronger feedback regime, $\kappa > 2.5 \times 10^7$ s^{-1}, as the feedback strength was fixed, both the frequency of the sinusoidal waveform and the oscillation frequency difference between the two observed modes varied with the delay time. Fig. 8 shows power spectra and oscillation spectra of the laser output for different delay times, where $\kappa = 5.5 \times 10^7$ s^{-1}. Fig. 8(a) is the power spectrum for a 10-m fiber with a delay time 10^{-7} s and Fig. 8(c) is the corresponding oscillation spectrum. Both the frequency of sinusoidal waveform and the oscillation frequency difference between two modes are 5.8 MHz. Fig. 8(b) shows the power spectrum for a 2-m fiber (corresponding delay time: 2×10^{-8} s) and Fig. 8(d) is the oscillation spectrum, while both the frequency of sinusoidal waveform and the oscillation frequency difference

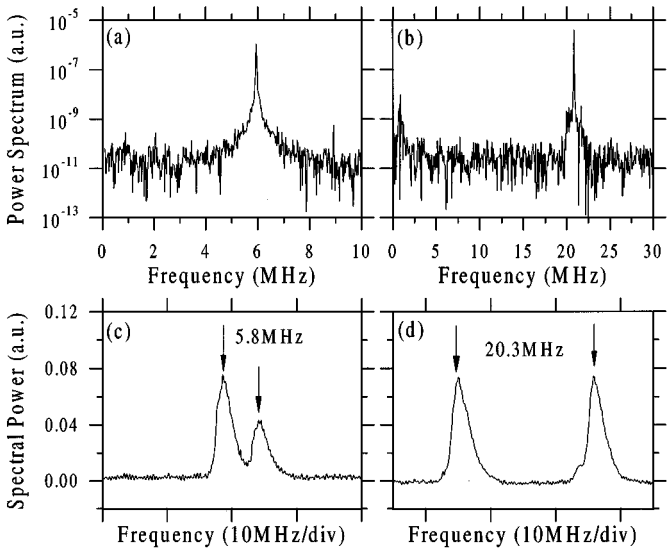

Fig. 8. Power spectra and oscillation spectra of laser output with different delay times, where $\kappa = 5.5 \times 10^7\ \mathrm{s}^{-1}$. (a), (c) A 10-m fiber which corresponds to a delay time of 10^{-7} s. (b), (d) A 2-m fiber (2×10^{-8} s). The frequency difference of the two oscillation modes is indicated by the down arrows.

between two modes are 20.3 MHz. The frequency of the sinusoidal waveform coincides with the oscillation frequency difference between two observed modes and they are vary inversely with the delay time when the coupling coefficient is fixed. Because the scanning rate of the scanning Fabry–Perot is 30 Hz, the oscillation spectra were measured in an average of 1/30 s; how these two modes interact with each other could not be specified by the measurements. However, these measurements strongly suggest that these two observed modes are nothing other than external cavity modes [which can be derived from (5)] of the compound cavity to be discussed in the next section. Note that the mode spacing does not coincide with the simple free-spectral range of the external cavity. Furthermore, the nonlinear interaction between the two stable external cavity modes is considered to result in large-amplitude sinusoidal oscillations.

Although the results reported above were for a pumping power at 88 mW, exactly the same dynamics were observed independently of the pumping power levels in a single-mode regime. In short, in LD-pumped Nd:YVO_4 microchip single-mode laser with fiber feedback, two different kinds of instability, i.e., random switching between noise-driven relaxation oscillation and chaotic spike oscillation (random chaotic burst state) and random switching between noise-driven relaxation oscillation and large-amplitude sinusoidal oscillation (random sinusoidal burst state) were observed for different feedback strengths. In the next section, we will explore the observed dynamics based on the Lang–Kobayashi model.

IV. Theoretical Exploration Based on the Lang–Kobayashi Model

A. General Characteristics of the Lang–Kobayashi Model

Since our system is essentially a single-mode laser with weak feedback, we employed the Lang–Kobayashi model [1] to explore the dynamics. We used the normalized Lang–Kobayashi equations with Langevin noise sources [20], [29], [30]

$$\frac{dS(t)}{dt} = K\{[N(t)-1]S(t)\} + 2\kappa\sqrt{S(t)S(t-T)}\cos\Theta(t) + F_S(t) \quad (2)$$

$$\frac{dN(t)}{dt} = W - N(t) - N(t)S(t) + F_N(t) \quad (3)$$

$$\frac{d\phi(t)}{dt} = \Delta\omega + \frac{1}{2}\alpha K[N(t)-1] - \kappa\sqrt{\frac{S(t-T)}{S(t)}}\sin\Theta(t) + F_\phi(t) \quad (4)$$

where $\Theta(t) = \omega T + \phi(t) - \phi(t-T)$ and $\omega = \omega_{\mathrm{th}} + \Delta\omega$ is the optical angle frequency of the solitary laser, ω_{th} is the optical angular frequency of solitary laser near threshold, and $\Delta\omega$ is the optical angular frequency shift of the laser deviated from the threshold. Equations (2)–(4) are the temporal evolution equations for the photon density S, the slowly varying part of the optical phase ϕ, and the population inversion density N. In the rate equations, t has been normalized to τ_f. $W = P/P_{\mathrm{th}}$ is the normalized pumping rate, K is the time ratio between τ_f and τ_S, α is linewidth enhancement factor, T is the delay time, and Θ is the phase difference between the output and the feedback beams [33]. F_S, F_N, and F_ϕ are the Langevin noise sources which satisfy $\langle F_i(t)\rangle = 0$ and $\langle F_i(t)F_j(t')\rangle = 2D_{ij}\delta(t-t')$. The angle brackets denote a time average and D_{ij} is the diffusion coefficient associated with the corresponding noise source. Here, the subscripts $i, j = S, N, \phi$. Their explicit expressions are

$$D_{SS} = \varepsilon S, \quad D_{\phi\phi} = \frac{\varepsilon}{(4S)}, \quad D_{S\phi} = 0$$
$$D_{NN} = \varepsilon S + N, \quad D_{SN} = -\varepsilon S, \quad D_{N\phi} = 0$$

where ε is the spontaneous emission coefficient. The stationary solutions of (2)–(4) are external cavity modes. The stationary optical angular frequency is the solution of

$$\Delta\omega T + C\sin(\omega T + tan^{-1}\alpha) = 0 \quad (5)$$

where $C \equiv \kappa T\sqrt{1+\alpha^2}$ is called effective feedback strength. The linewidth enhancement factor α in LDs stems from the combined effect of free-carrier plasma effect and detuning effect of lasing frequency from the spontaneous emission peak, i.e., the Kramers–Kronig relationship. In microchip solid-state lasers, no one has determined its value experimentally. However, recent experimental demonstration of large phase-conjugate reflection from Nd:YVO_4 lasers operating near gain peak [32] indicates that the Nd:YVO_4 laser itself has a substantially large χ^3 nonlinearity which is directly related to a α-nonlinearity in the form of $\chi^3 = (\alpha - j)(G_0/I_s)$ where

G_0 small-signal gain;
I_s saturation intensity
j $= \sqrt{-1}$.

Therefore, we will use a nonzero α in the simulation. The steady-state characteristics can be characterized by C. From

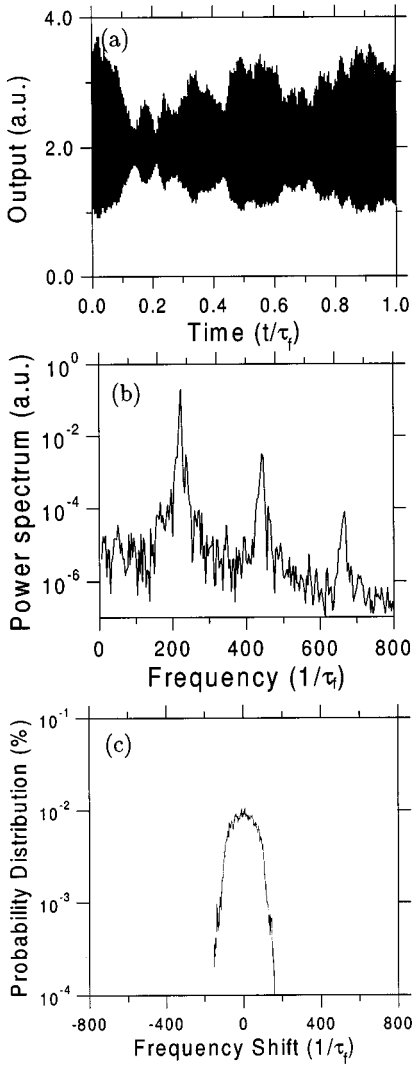

Fig. 9. Typical numerical characteristics of $S(t)$ based on the Lang–Kobayashi model with $\kappa = 0$. (a) Temporal waveform. (b) Power spectrum. (c) Oscillation frequency histogram.

(5), the number of steady-state solutions increases as κ or T increases. As κ or T is increased, new external cavity modes are created in pairs after saddle-node bifurcation. The results are: if $C < 1$, there is only one external cavity mode such that the laser cavity mode is minimally perturbed by the external cavity. On the other hand, for $C > 1$, there are $2n + 1$ external cavity modes in total, where n is an integer. It can be verified that the stability condition follows as

$$1 + Ccos(\omega T + tan^{-1}\alpha) > 0. \tag{6}$$

As (6) does not hold, the solution is intrinsically unstable (i.e., a saddle point) and is called antimode [22]. However, it should be noted that external cavity modes are not always dynamically stable even if this quantity is positive [33] and their stabilities change depending on $\Delta\omega T$ in (5). In short, dynamical stability of an external cavity mode depends critically on the solitary laser frequency $\omega_{\rm th}$ in a large delay case as in our present experiment.

The linewidth in the presence of external feedback is approximately given by [34]

$$(\Delta\nu)_f \simeq \frac{\Delta\nu}{[1 + Ccos(\omega T + tan^{-1}\alpha)]^2} \tag{7}$$

where $\Delta\nu$ is the solitary laser linewidth. Equation (7) shows that, depending upon the feedback phase ωT, the laser linewidth can broaden or narrow. The maximum narrowing occurs when $\omega T + tan^{-1}\alpha = 2m\pi$, where m is an integer, and the reduction factor in that case is $(1 + C)^2$. Clearly the linewidth can be reduced considerably for a large value of C if the external cavity length is fine-tuned to adjust ωT. Reductions by more than three orders of magnitude have been observed [35]. As discussed earlier, when $C > 1$, there are multiple external cavity modes over which the laser can be made to oscillate by changing the external cavity length [36]. In the case of mode hopping, the linewidth can vary by a large amount with little change in T [37]. For $C < 1$, only one external cavity mode oscillates for all values of the phase. Considerable linewidth broadening can occur in this case for certain range of phase values, as seen clearly by an inspection of (7). However, (7) is very sensitive to the feedback phase ωT. For the parameters of our experimental condition, i.e., $\lambda_0 = 1064.245$ nm, $\omega T \approx (1.18 \times 10^7 \times L)$ rad, where L is the effective external cavity length. Even a 1-μm variation of the effective external cavity length can vary ωT for 7.7 rad. We did not fine-tune this value in the experiments. Instead, we just paid attention to the change of the lasing linewidth as instabilities occurred. Nevertheless, we did not observe any significant linewidth narrowing. On the other hand, linewidth broadening with a maximum $(\Delta\nu)_f/\Delta\nu \sim 2.5$ occurred only when chaotic spike oscillation appeared.

The chief difference between solid-state lasers and LDs are the time scales. The relevant time scales in our laser system are: $\tau_f = 90 \times 10^{-5}$ s, $\tau_S \sim 2 \times 10^{-10}$ s, $f_{RO} \sim 1.7$ MHz, decay time $\sim 8.76 \times 10^{-5}$ s, the internal round-trip time $= 1.33 \times 10^{-11}$ s for a 1-mm-thick crystal, and the external round-trip time $= 3.3 \times 10^{-8}$ s for a 5-m fiber. According to these parameters, it is worthwhile to note that there are two significant differences between solid-state lasers and LDs. First, the lifetime ratio K for a solid-state laser is about $10^5 - 10^7$ and 10^3 for LDs. Second, in solid-state laser, the round-trip time is usually larger than the reciprocal of f_{RO} whereas in LDs, in most cases, it is smaller than the reciprocal of f_{RO}. It is conjectured that these two differences are the primary reasons that result in the different behaviors between solid-state lasers and LDs with feedback.

We solved (2)–(4) numerically by the Heun method [38]. The parameters used here are: $W = 3\tau_f^{-1}$, $K = 10^6\tau_f^{-1}$, $\alpha = 2$, $\omega_{th} = 1.6 \times 10^{11}$ radτ_f^{-1}, $\Delta\omega = 10$ radτ_f^{-1}, $D_{SS} = 5 \times 10^{-9}\tau_f^{-2}$, $D_{NN} = 5 \times 10^{-9}\tau_f^{-2}$, $D_{\phi\phi} = 2 \times 10^6$ rad$^2\tau_f^{-2}$ and $T = 0.001\tau_f$. The corresponding fiber length is about 9 m. To explain the experimental results, such as feedback-induced instabilities and linewidth broadening, we shall introduce a relatively large phase (i.e., FM) noise. The large phase noise derives from the spontaneous emission. Nd:YVO_4 lasers contain larger spontaneous emission noise so that they exhibit larger linewidth than other solid state lasers. The linewidth of the solitary Nd:YVO_4 laser is about 2 MHz, whereas that of

single-mode LNP lasers is only about few hundred kilohertz. As a result, the following results could not be reproduced in a single-mode domain of LNP lasers even if a corresponding feedback strength was included. The phase noise we use corresponds to the linewidth of the Nd:YVO_4 laser.

A typical temporal waveform, power spectrum, and oscillation frequency histogram for a solitary laser, i.e., $\kappa = 0$, are shown in Fig. 9. Here, the oscillation frequency histogram was calculated based on (4), i.e., $d\phi(t)/dt = \delta\omega(t)$, by using the numeric of simulated $S(t)$, $N(t)$, and $\phi(t)$. $\delta\omega(t)$ is the laser optical angular frequency fluctuation as a function of time. The probability distribution of $\delta\omega(t)$ is plotted. The histogram may correspond to the oscillation spectrum qualitatively. The correspondence between the experiment and the simulation is fine. The numerical temporal waveform of $S(t)$ of a solitary laser shown in Fig. 9(a) indicates noise-driven relaxation oscillation with amplitude fluctuations similar to the experimental results reported in Fig. 2(a). In the power spectrum, shown in Fig. 9(b), f_{RO} at $210\tau_f^{-1}$ and its high-order harmonic can be recognized. When we increase W, f_{RO} also increases. A typical oscillation frequency histogram is shown in Fig. 9(c).

B. Weaker Feedback Strength ($\kappa = 10\tau_f^{-1}$)

Optical feedback was introduced with $\kappa \neq 0$. When κ was small, the temporal waveform, the power spectrum, and the oscillation frequency histogram were still similar to those of a solitary laser. This parallels the experimental observation. When $\kappa = 10\tau_f^{-1} \approx 1.1 \times 10^5$ s^{-1} (assuming $\tau_f = 90$ μs) and by tuning the $\omega_{\rm th}$ value precisely, the sustained relaxation oscillation spiking appeared in the absence of phase noise as shown in Fig. 10(a). Here, we assumed a negligibly small carrier density noise D_{NN} and a photon density noise D_{SS} of $5 \times 10^{-9}\tau_f^{-2}$. Therefore, the resulting spiking oscillations are considered to be a deterministic instability resulting from weak optical feedback. However, this spike oscillation persists, and no bursting occurs in the absence of phase noise.

When we introduced phase noise whose magnitude is relevant to that of the linewidth of the Nd:YVO_4 laser, the random chaotic burst state was reproduced quite well. An example is shown in Fig. 10(b), assuming $D_{\phi\phi} = 2 \times 10^6$ rad$^2\tau_f^{-2}$. The output waveform switches randomly between noise-driven relaxation oscillation and chaotic spike oscillation. The corresponding power spectra and the oscillation frequency histogram are shown in Fig. 11. As Fig. 11(a) shows, the f_{RO} of noise-driven relaxation oscillation is about $210\tau_f^{-1}$ which is equal to that of the solitary laser. For chaotic spike oscillation, as shown in Fig. 11(b), the main frequency component shifts to a lower value (around at $190\tau_f^{-1}$) and the broad-band characteristic is also observed. The linewidth broadened to three times as the chaotic burst occurred as shown in Fig. 11(c) and (d). This is similar to the experimental results shown in Fig. 4.

Under the present setting of parameters, f_{RO} as well as the main frequency component of chaotic spike oscillation also decreased as κ was increased. This result is different from that in LDs with feedback. Because the main difference between the LD and the solid-state laser are the dynamic time scales, we used another set of time scales for the LD, i.e., $K = 10^3$ and $\tau_f = 10^{-9}$ s, and fixed all other parameters. For these new time scale settings, f_{RO} increases with a increase of κ. From these results, the different trend of the dependence of f_{RO} on κ is due to the different dynamical time scales.

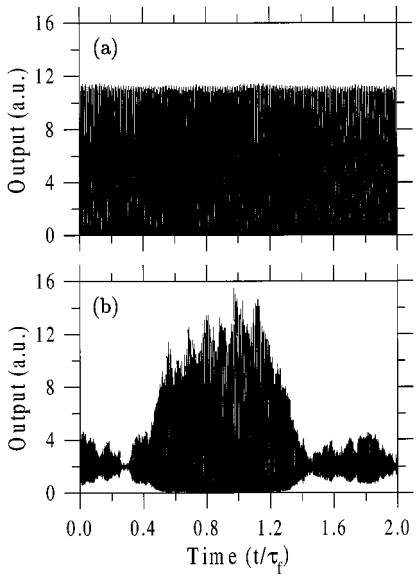

Fig. 10. Numerical temporal waveform of $S(t)$ with $\kappa = 10\tau_f^{-1}$. (a) Without phase noise, $D_{\phi\phi} = 0$. (b) With phase noise, $D_{\phi\phi} = 2 \times 10^6$ rad$^2\tau_f^{-2}$.

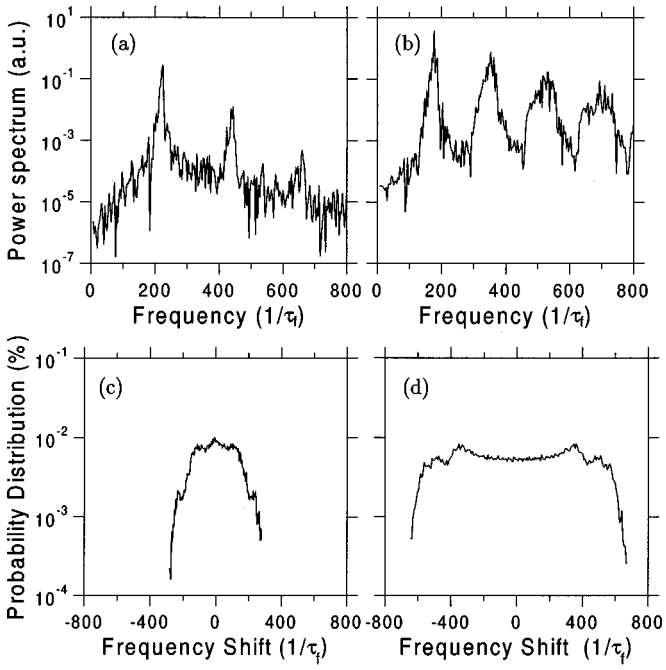

Fig. 11. Corresponding power spectra and oscillation frequency histogram of Fig. 10(b). (a), (c) Noise-driven relaxation oscillation. (b), (d) Chaotic spike oscillation.

From these quantitative agreements between the experiment and the numerical results in all aspects, the chaotic bursting can be concluded to appear due to phase fluctuation of the laser (i.e., FM noise), which corresponds to fluctuations of $\omega_{\rm th}$. In short, random chaotic burst is thought to be random dynamic switchings between the unstable state and the stable state driven by FM noise [39].

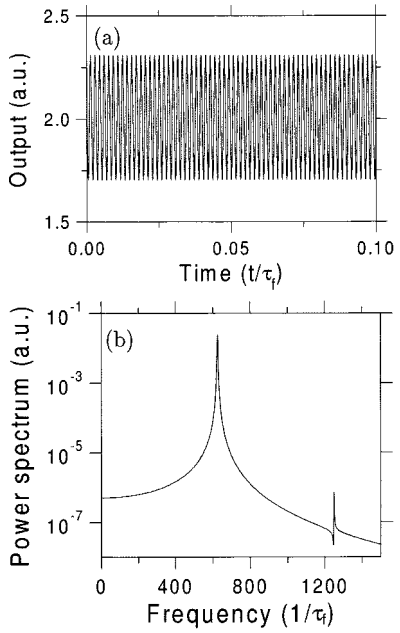

Fig. 12. (a) Numerical temporal waveform of $S(t)$ and (b) its power spectrum for $\kappa = 2000\tau_f^{-1}$, where the phase noise is removed , i.e., $D_{\phi\phi} = 0$.

Let us evaluate the corresponding effective feedback parameter C in the present system. For the condition of numerical simulation, $\kappa = 10\tau_f^{-1}$ and thus $C = 0.022$, which is smaller than 1. Therefore, only one external cavity mode interacts with the solitary laser mode. In our experiment, for the case of weak feedback, i.e., $\kappa = 10^6\ \mathrm{s}^{-1}$, $C = 0.071$, which is also smaller than 1. According to the context of LDs with feedback described by the single-mode Lang–Kobayashi equation, no low-frequency fluctuations instability should happen in the regime where C is smaller than 1. Nevertheless, in the case of microchip solid-state lasers in a large delay limit, the instabilities can be excited due to intrinsic phase noise in lasers.

C. Stronger Feedback Strength ($\kappa = 2000\tau_f^{-1}$)

In the experiments, when the feedback strength is stronger, random sinusoidal burst and two operation modes were observed. The frequency of large-amplitude sinusoidal oscillation and the frequency separation of the two observed modes coincide.

We first increased the coupling strength to $2000\tau_f^{-1}$ and turned off the phase noise. A sinusoidal waveform was easily obtained. An example is shown in Fig. 12. From the calculated power spectrum of the sinusoidal waveform, the frequency is determined to be about $620\tau_f^{-1}$. Just as the large-amplitude sinusoidal waveform observed in the experiment with stronger feedback, the amplitude of the sinusoidal waveform is several times larger than the fluctuation amplitude of the noise-driven relaxation oscillation and the frequency of the sinusoidal waveform is also several times larger than f_{RO}. When we increased κ, the frequency of the sinusoidal waveform also increased. This means that when coupling strength increases another deterministic state appears, sustaining large-amplitude sinusoidal oscillation and replacing the RO state.

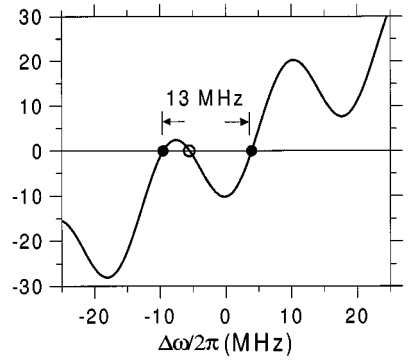

Fig. 13. Determination of external cavity modes based on a graphical solution of (5) assuming $C = 3.65$, $\omega = 1.77 \times 10^{15}$ rad/s, $\alpha = 1$, and $T = 5.6 \times 10^{-8}$ s. The solid circles denote stable solutions and the empty circle denotes the unstable solution. The frequency difference between the two stable solutions is 13 MHz.

Apparently, the experimentally observed random sinusoidal burst is a kind of random switch between the two states, i.e., the sustained large-amplitude sinusoidal oscillation and noise-driven relaxation oscillation. However, in numerical simulations, we cannot reproduce the observed bursts. To be more specific, only the degradation of the sinusoidal waveforms were numerically obtained and no switching was achieved even with an increase of the phase noise. This behavior is totally different from the numerical result of random chaotic burst in the weakly-coupled regime, in which clear switching takes place.

Although a direct numerical verification has not been achieved, some analytical pictures provide the mechanism. As mentioned above, when $C < 1$, there is only one external cavity mode solution, while for $C > 1$ multiple external cavity mode solutions appear. In the experiments, in the case of stronger feedback with $\kappa = 5.5 \times 10^7\ \mathrm{s}^{-1}$, $C \sim 3.65 > 1$. Multiple solutions are expected in such a stronger feedback condition. Since (5) is a transcendental equation, we solved it graphically with the following parameters: $C = 3.65$, $\omega = 1.77 \times 10^{15}$ rad/s, $\alpha = 1$, and $T = 5.6 \times 10^{-8}$ s. Based on the stability analysis of (6), the solutions of (5) are determined graphically as shown in Fig. 13, in which $\Delta\omega/2\pi$ is the optical frequency shift. Referring to Fig. 13, the solid circles denote the external cavity mode solutions while the empty ones denotes the saddle (antimode). The oscillation frequency separation of the two stable external cavity mode solutions is about 13 MHz, which is close to the experimental result. This implies that the two observed modes measured by the scanning Fabry–Perot interferometer are nothing other than the external cavity modes described above. From (5), it is also easy to show that the frequency spacing of the two stable external cavity modes increases with an increase of the coupling strength as well as the delay time. The value ranges from 0, for single-mode operation, to $c/2nL$, for very strong coupling strength.

When multiple external cavity modes were allowed to exist in the laser system, mode hopping between these external cavity modes is expected to happen. Furthermore, complex nonlinear dynamic behavior due to the interaction between these external cavity modes was also expected. Therefore, large-amplitude

sinusoidal wave generation is considered to arise through the nonlinear interaction between these two external cavity modes. There are two possibilities which may explain random switching of this sinusoidal waveform observed in the experiment. One is the noise-induced switching between a one-external cavity mode state and a two-external cavity mode state, in which a sinusoidal waveform appears. Another explanation is that the switching occurs "deterministically," reflecting the self-induced fluctuation of the external cavity length through the intensity-dependent self-phase modulation in the fiber in the strongly coupled regime, which is not included in (2)–(4).

V. Conclusion

In our experiments, two kinds of instabilities were observed in an LD-pumped microchip Nd:YVO_4 single-mode laser with fiber feedback in different feedback strength regimes. Random switching between noise-driven relaxation oscillation and chaotic spike oscillation was observed in the weaker feedback regime, $\kappa = 1.1 \times 10^5$ s^{-1}–2.5×10^7 s^{-1}. In this regime, the main frequency component in the power spectrum was shifted to a lower value and the lasing linewidth broadened as chaotic spiking appeared. In LDs with external feedback, linewidth broadening or narrowing were observed under certain experimental conditions. However, this linewidth variation is very sensitive to the effective cavity length L. Here, we focused only on what happened to the laser linewidth when instabilities occurred and only linewidth broadening was observed with a concurrent appearance of chaotic spike oscillation. Employing the single-mode Lang–Kobayashi equations, the random-switching waveform between noise-driven relaxation oscillation and chaotic spike oscillation as well as the power spectrum frequency shift and linewidth broadening have been reproduced successfully by including a relevant phase noise in the Nd:YVO_4 laser.

In a stronger feedback regime, $\kappa = 2.5 \times 10^7$ s^{-1}–1.7×10^8 s^{-1}, the random switching between noise-driven relaxation oscillation and large-amplitude sinusoidal oscillation was observed. Two operational modes appear randomly in the oscillation spectrum and the oscillation frequency difference between the two observed modes almost coincide with the frequency of large-amplitude sinusoidal oscillation. In contrast to the weakly-coupled regime, we did not observe any significant linewidth broadening or narrowing in this regime. The sinusoidal waveform with a frequency value approximately equal to the oscillation frequency spacing between two stable external cavity modes was confirmed by graphical solutions of external cavity modes and numerical simulations of the single-mode Lang–Kobayashi equations together with large coupling coefficient and zero phase noise. However, with the present parameter setting, we cannot reproduce the sinusoidal burst. Further investigations over a wider region of parameters and the effect of intensity-dependent self-phase modulation in the optical fiber are under progress.

The linewidth enhancement factor, α, is an important parameter here. Although there is no experimental measurement to determine the values in microchip solid-state lasers, due to the substantially large χ^3 nonlinearity of Nd:YVO_4 itself, as shown in [31], we assumed a nonzero value in simulations and obtained good agreement with the experiment.

Finally, we would like to emphasize that the observed instabilities are totally different from the instabilities in LDs. The phase-noise-driven chaotic spiking instability occurred in a very weak feedback strength regime, which is thought to be stable in LDs. In this regime, phase noise plays an important role. In the stronger feedback regime, random sinusoidal burst, which as to our knowledge, has also not been observed in LDs. It is worthwhile to note that the delay time due to optical feedback is larger than the characteristic time scale of microchip solid-state lasers. However, for the case of LDs, the delay time is usually smaller than the characteristic time scale of LDs. The peculiar differences in time scales bring out unique dynamical features for solid-state lasers with optical feedback which are significantly different from that of LDs with optical feedback.

References

[1] R. Lang and K. Kobayashi, "External optical feedbacl effects on semiconductor injection laser properties," *IEEE J. Quantum Electron.*, vol. QE-16, pp. 347–355, 1980.

[2] K. Petermann, "External optical feedback phenomena in semiconductor lasers," *IEEE J. Select. Topics Quantum Electron.*, vol. 1, pp. 480–489, 1995.

[3] A. T. Ryan and G. P. Agrawal, "Optical-feedback-induced chaos and its control in multimode semiconductor lasers," *IEEE J. Quantum Electron.*, vol. 30, pp. 668–679, 1994.

[4] B. W. Liby and D. Statman, "Controling the linewidth of a semiconductor laser with photorefractive phase conjugate feedback," *IEEE J. Quantum Electron.*, vol. 32, pp. 835–838, 1996.

[5] N. Kikuchi, Y. Liu, and J. Ohtsubo, "Chaos control and noise suppression in external-cavity semiconductor lasers," *IEEE J. Quantum Electron.*, vol. 33, pp. 56–65, 1997.

[6] S. I. Turovets, J. Dellunde, and K. A. Shore, "Nonlinear dynamics of a laser diode subjected to both optical and electronic feedback," *J. Opt. Soc. Amer. B*, vol. 14, pp. 200–208, 1997.

[7] J. Wieland, C. R. Mirasso, and D. Lenstra, "Prevention of coherence collapse in diode lasers by dynamic targeting," *Opt. Lett.*, vol. 22, pp. 469–471, 1997.

[8] Y. Kitaoka, H. Sato, K. Mizuuchi, K. Yamamoto, and M. Kato, "Intensity noise of laser diodes with optical feedback," *IEEE J. Quantum Electron.*, vol. 32, pp. 822–828, 1996.

[9] P. Kürz and T. Mukai, "Frequency stabilization of a semiconductor laser by external phase-conjugate feedback," *Opt. Lett.*, vol. 21, pp. 1369–1371, 1996.

[10] C. R. Mirasso, P. Colet, and P. Garcia-Fernandez, "Synchronization of chaotic semiconductor lasers: Application to encoded communications," *IEEE Photon. Technol. Lett.*, vol. 8, pp. 299–301, 1996.

[11] V. Annovazzi-Lodi, S. Donati, and A. Scire, "Synchronization of chaotic injected-laser systems and its application to optical cryptography," *IEEE J. Quantum Electron.*, vol. 33, pp. 953–959, 1996.

[12] J. Martin-Regalado, G. H. M. van Tartwijk, S. Balle, and M. S. Miguel, "Mode control and pattern stabilization in broad-area laser by optical feedback," *Phys. Rev. A*, vol. 54, pp. 5386–5393, 1996.

[13] M. Homar, J. V. Moloney, and M. S. Miguel, "Travelling wave model of a multimode Fabry-Perot laser in free running and external cavity configurations," *IEEE J. Quantum Electron.*, vol. 32, pp. 553–566, 1996.

[14] J. Dellunde, M. C. Torrent, C. R. Mirasso, E. Hernandez-Garcia, and J. M. Sancho, "Analytical calculations of switch-on time and timing jitter in diode lasers subjected to optical feedback and external light injection," *Opt. Commun.*, vol. 115, pp. 523–527, 1995.

[15] G. H. M. van Tartwijk and M. S. Miguel, "Optical feedback on self-pulsating semiconductor lasers," *IEEE J. Quantum Electron.*, vol. 32, pp. 1191–1202, 1996.

[16] K. Otsuka, "Ultrahigh sensitivity laser Doppler velocimetry with a michrochip solid-state laser," *Appl. Opt.*, vol. 33, pp. 1111–1114, 1994.

[17] ——, "Laser-fluctuation measurements in a bath of strong Gaussian noise," *Appl. Phys.*, vol. 18, pp. 415–419, 1979.

[18] K. Otsuka, J.-Y. Ko, J.-L. Chern, K. Ohki, and H. Utsu, "Instabilities in a laser-diode-pumped microchip solid-state laser with feedback," *Phys. Rev. A*, vol. 60, pp. R3389–R3392, 1999.

[19] J. Mørk, B. Tromborg, and P. L. Christiansen, "Bistability and low-frequency fluctuations in semiconductor lasers with optical feedback: A theoretical analysis," *IEEE J. Quantum Electron.*, vol. QE-24, pp. 123–133, 1988.
[20] A. Hohl, H. J. C. van der Linden, and R. Roy, "Determinism and stochasticity of power-dropout events in semiconductor lasers with optical feedback," *Opt. Lett.*, vol. 20, pp. 2396–2398, 1995.
[21] C. H. Henry and R. F. Kazarinov, "Instability of semiconductor lasers due to optical feedback from distant reflectors," *IEEE J. Quantum Electron.*, vol. QE-22, pp. 294–301, 1986.
[22] T. Sano, "Antimode dynamics and chaotic itinerancy in the coherence collapse of semiconductor lasers with optical feedback," *Phys. Rev. A*, vol. 50, pp. 2719–2726, 1994.
[23] G. H. M. van Tartwijk, A. M. Levine, and D. Lenstra, "Sisyphus effect in semiconductor lasers with optical feedback," *IEEE J. Select. Topics Quantum Electron.*, vol. 1, pp. 466–472, 1995.
[24] I. Fischer, G. H. M. van Tartwijk, A. M. Levine, W. Elsässer, E. Göbel, and D. Lenstra, "Fast pulsing and chaotic itenerancy with a drift in coherence collapse of semiconductor lasers," *Phys. Rev. Lett.*, vol. 76, pp. 220–223, 1996.
[25] G. Huyet, S. Balle, M. Giudici, C. Green, G. Giacomelli, and J. R. Tredicce, "Low frequency fluctuations and multimode operation of a semiconductor laser with optical feedback," *Opt. Commun.*, vol. 149, pp. 341–347, 1998.
[26] K. Petermann, *Laser Diode Modulation and Noise*. Norwell, MA: Kluwer, 1991, pp. 251–252.
[27] J.-S. Lih, J.-Y. Ko, J.-L. Chern, and I.-M. Jiang, "Determinism test and noise estimate for a complex time series," *Europhys. Lett.*, vol. 40, pp. 7–12, 1997.
[28] H. Temkin, N. A. Olsson, J. H. Abeles, R. A. Logan, and M. B. Panish, "Reflection noise in index-guided InGaAs lasers," *IEEE J.Quantum Electron.*, vol. QE-22, pp. 286–293, 1986.
[29] K. Petermann, *Laser Diode Modulation and Noise*. Norwell, MA: Kluwer, 1991, pp. 267–269.
[30] J. Ohtsubo, "Feedback induced instability and chaos in semiconductor lasers and their applications," *Opt. Rev.*, vol. 6, pp. 1–15, 1999.
[31] G. P. Agrawal and N. K. Dutta, *Semiconductor Lasers* . New York: Van Nostrand Reinhold, 1993, pp. 259–260.
[32] A. Brignon, L. Loiseau, C. Larat, J.-P. Huignard, and J.-P. Pocholle, "Phase conjugation in a continuous-wave diode-pumped Nd:YVO_4 laser," *Appl. Phys. B*, vol. 69, pp. 159–162, 1999.
[33] G. P. Agrawal and N. K. Dutta, *Semiconductor Lasers* . New York: Van Nostrand Reinhold, 1993, pp. 304–306.
[34] G. P. Agrawal, "Line narrowing in a single-mode injection laser due to external optical feedbck," *IEEE J. Quantum Electron.*, vol. QE-20, pp. 468–471, 1984.
[35] R. Wyatt and W. J. Delin, "10 kHz linewidth 1.5 μm InGaAsP external cavity laser with 55 nm tuning range," *Electron. Lett.*, vol. 19, pp. 110–112, 1983.
[36] G. A. Acket, D. Lenstra, A. J. den Boef, and B. H. Verbeek, "The influence of feedback intensity on longitudinal mode propertise and optical noise in index-guided semiconductor lasers," *IEEE J. Quantum Electron.*, vol. QE-20, pp. 1163–1170, 1984.
[37] E. Patzak, H. Olesen, A. Sugimura, S. Saito, and T. Mukai, "Spectral linewidth reduction in semiconductor lasers by an external cavity with weak optical feedback," *Electron. Lett.*, vol. 19, pp. 938–940, 1983.
[38] J. Honerkamp, *Stochastic Dynamical System* . New York: VCH, 1994, pp. 294–295.
[39] K. Otsuka, *Nonlinear Dynamics in Optical Complex Systems*. Norwell, MA: Kluwer, 2000, pp. 175–185.

Tsong-Shin Lim was born in Changhua, Taiwan, R.O.C., in 1974. He received the B.S. and M.S degrees in physics from the National Cheng Kung University, Tainan, Taiwan, in 1996 and 1998, respectively, where he is currently working toward the Ph.D. degree, and is engaged in research of nonlinear dynamics in laser systems.

Mr. Lim is a member of the American Physical Society and the Optical Society of America.

Tsung-Hsun Yang was born in Taipei, Taiwan, R.O.C., in 1966. He received the M.S. degree in physics from the National Tsing Hua University, Hsinchu, Taiwan, in 1990 and the Ph.D. degree in electro-optics engineering from the National Chiao Tung University, Hsinchu, Taiwan, in 1998.

From 1998 to 2000, he was with the Department of Physics, National Cheng Kung University, Tainan, Taiwan, as a post-doctoral Fellow. In 2000, he joined the Institute of Electro-optics, National Chiao Tung Univeristy as a post-doctoral Fellow. His current research interests include the optical communications and the stochastic resonance phenomena in nonlinear dynamical systems.

Jyh-Long Chern was born in Kaohsiung, Taiwan, R.O.C., in 1961. He received the B.S. and M.S. degrees in physics, both from the National Tsing Hua University, Hsinchu, Taiwan, in 1984 and 1986, respectively, and the Ph.D. degree in optical science from the University of New Mexico at Albuquerque in 1991.

From 1986 to 1988, he was engaged in compulsory army service. In 1991, he joined NTT Basic Research Laboratories, Nippon Telegraph and Telephone Corporation, as a post-doctoral Fellow. From 1992 to 1995, he was with the Department of Physics, National Sun Yat-Sen University, Kaohsiung, Taiwan, as an Associate Professor, later promoted to a Full Professor in 1995. In 1996, he transferred to the Department of Physics, National Cheng Kung University, Tainan, Taiwan. He has published over 50 journal papers. His major fields of research are nonlinear dynamics and optical physics.

Kenju Otsuka (A'68–M'78–SM'80–F'94) was born in Manchuria, Japan, in 1946. He received the B.S. and Ph.D. degrees from Tohoku University, Sendai, Japan, in 1968 and 1976, respectively.

In 1968, he joined the Musashino Electrical Communication Laboratories, Nippon Telegraph and Telephone Public Corporation (presently NTT). He was engaged in the basic research of lasers, ultrafast optical pulse generation, photonic devices, and nonlinear dynamics in optical systems. From 1981 to 1982, he was with the Edward L. Ginzton Laboratory, Stanford University, Stanford, CA, as a Guest Scientist. In 1994, he transferred to the Department of Applied Physics, School of Engineering, Tokai University, Kanagawa, Japan, as a Professor. He also serves as a Visiting Professor at Universitè Libre de Bruxelles, Brussels, Belgium. Currently, he is Head of the Department of Human and Information Science, Tokai University, and is engaged in the research of laser-diode-pumped microchip lasers and nonlinear dynamics in optical systems, as well as their applications. His contributions include three book chapters and authoring the monograph *Nonlinear Dynamics in Optical Complex Systems* (Dordrecht, The Netherlands: Kluwer, 1999).

Dr. Otsuka is a member of the Physical Society of Japan, the Japan Society of Applied Physics, the American Physical Society, and is a Fellow of the Optical Society of America.